Available online at www.sciencedirect.com
SCIENCE DIRECT®
International Journal of Heat and Mass Transfer 47 (2004) 1719–1730
International Journal of HEAT and MASS TRANSFER
www.elsevier.com/locate/ijhmt

Effect of fin waviness and spacing on the lateral vortex structure and laminar heat transfer in wavy-plate-fin cores

Jiehai Zhang, Jaydeep Kundu, Raj M. Manglik *

Thermal-Fluids & Thermal Processing Laboratory, Department of Mechanical, Industrial and Nuclear Engineering, University of Cincinnati, 598 Rhodes Hall, P.O. Box 210072, Cincinnati, OH 45221-0072, USA

Received 23 July 2003; received in revised form 17 October 2003

Abstract

Laminar forced convection in air ($Pr = 0.7$) in two-dimensional wavy-plate-fin channels with sinusoidal wall corrugations is numerically simulated. Constant property, periodically developed flow in uniform wall temperature plate channels is considered. Velocity and temperature fields, isothermal Fanning friction factor, and Colburn factor are presented for different flow rates ($10 \leqslant Re \leqslant 1000$), wall-corrugation severity ($0.125 \leqslant \gamma \leqslant 0.5$), and fin spacing ($0.1 \leqslant \varepsilon \leqslant 3.0$). Lateral vortices or re-circulation cells develop in the wavy-wall troughs as the axial flow gets separated downstream of the wall-corrugation peaks and re-attaches upstream of the subsequent wall peak, and their strength and coverage is a function of Re, γ, and ε. As the plate separation ε decreases, however, viscous forces dominate and dampen the swirl; with very large ε, the impact of wall waviness diminishes and the core fluid flows largely undisturbed. The surface waviness-induced periodic disruption and thinning of boundary layers along with lateral swirl mixing produce high local heat fluxes near the wall peak regions. The overall heat transfer coefficient increases many fold compared to that in flat-plate channels with relatively small increases in the concomitant pressure drop penalty. The optimum (j/f) enhancement is obtained in the swirl flow regime ($Re > 100$) with $\gamma > 0$ and $1.0 \leqslant \varepsilon \leqslant 1.2$.

1. Introduction

Extended or finned surfaces are widely used in compact heat exchangers to enhance heat transfer and reduce their size [1–3]. Often geometrically modified fins are incorporated, which, besides increasing the surface area density of the exchanger, also improve the convection heat transfer coefficient. Some examples of such enhanced surface compact cores include offset-strip fins, louvered fins, perorated fins, and corrugated or wavy fins [1–6]. Of these, wavy fins are particularly attractive for their simplicity of manufacture, potential for enhanced thermal–hydraulic performance, and ease of usage in both plate-fin and tube-fin type exchangers. Typical sinusoidal wavy plate-fins are depicted in Fig. 1(a), and their geometric attributes are described by the waviness amplitude A, pitch L, inter-fin spacing S, and fin height H, as shown in Fig. 1(b). Their dimensionless representation is given by the corrugation aspect ratio γ ($= 2A/L$), fin spacing ratio ε ($= S/2A$), and flow cross-section aspect ratio α ($= S/H$).

Several investigations have addressed the issue of forced convective heat and/or mass transport in wavy or corrugated-wall channels used in a variety of different applications. These include wavy plate-fin channels [7–12], corrugated tube-fin cores [13–15], wavy-plate oxygenators [16–18], and corrugated inter-plate channels in plate-and-frame heat exchangers [19–23]. The surface corrugations in these devices have consisted of triangular, sinusoidal, and trapezoidal profiles, and the flow behavior has been studied both experimentally and computationally. It has generally been observed that wall corrugations induce a steady vortex or swirl in low

* Corresponding author. Tel.: +1-513-556-5704; fax: +1-513-556-3390.
E-mail address: raj.manglik@uc.edu (R.M. Manglik).

0017-9310/$ - see front matter © 2003 Elsevier Ltd. All rights reserved.
doi:10.1016/j.ijheatmasstransfer.2003.10.006

Nomenclature

A	amplitude of wall waviness, Fig. 1(b) (mm)
A_h	projected or equivalent flat-plate heat transfer surface area (m^2)
B	dimensionless pressure gradient, Eq. (4)
Br	Brinkman number ($=\rho v u_m^2/k\Delta T$)
c_p	specific heat (J/kg K)
d_h	hydraulic diameter ($=2S$) (mm)
f	Fanning friction factor based on projected flat-plate surface area, Eq. (10)
H	Fin height, Fig. 1(b) (mm)
k	thermal conductivity (W/m K)
j	Colburn factor ($=Nu/RePr^{1/3}$)
L	pitch of fin waviness, Fig. 1(b) (mm)
Nu	Nusselt number based on projected flat-plate surface area, Eq. (11)
Pe	Peclet number ($=Re\cdot Pr$)
Pr	Prandtl number ($=\mu c_p/k$)
P	dimensionless local pressure, Eq. (4)
p	pressure (Pa)
p^*	local pressure (Pa)
Re	hydraulic-diameter-based Reynolds number ($=u_m d_h/v=2Re_S$)
Re_S	plate-spacing based Reynolds number ($=u_m S/v$)
S	fin spacing, Fig. 1(b) (mm)
S_ϕ	source terms, Eqs. (8a)–(8c)
T	temperature (K)
U, V	dimensionless axial and lateral velocity components
u, v	axial and lateral velocity components (m/s)
x, y	Cartesian coordinates

Greek symbols

α	flow cross-section aspect ratio ($=S/H$)
β	global pressure gradient (Pa/m)
ε	channel spacing ratio ($=S/2A$)
ϕ	dependent variables ($=U$, V, and θ, respectively)
Γ	dimensionless coefficient, Eq. (7)
γ	channel corrugation ratio ($=2A/L$)
v	dynamics viscosity (m^2/s)
θ	dimensionless temperature, Eq. (5)
ρ	density, (kg/m^3)
ω	geometrical parameter, Eq. (2b)
ξ, η	dimensionless body-fitted coordinates

Subscripts

b	bulk or mixed-mean value
c	pertaining to the cross-section area
i	at inlet conditions
m	mean or average value
o	at outlet conditions
w	at wall conditions

Reynolds number flows in the trough regions of the wavy wall. This results in flow mixing and boundary layer disruption and thinning, thereby significantly enhancing the heat and mass transfer. The majority of computational models have considered a two-dimensional characterization of the flow geometry, which is valid when the fin height is much larger than the inter-fin spacing ($H \gg S$ or $\alpha \to 0$; see Fig. 1(b)).

Nishmura et al. [16–18] have experimentally and numerically studied laminar flow mass transfer enhancement in two-dimensional wavy-plate channels by varying the pitch, amplitude, and the channel spacing in the range of $0.215 \leqslant \varepsilon \leqslant 1.33$ and $\gamma = 0.25$. Rush et al. [11] have experimentally investigated the flow behavior in wavy-plate channels with plate-spacing ratio $\varepsilon > 1.0$ and rather slender wall waviness ($0.172 \leqslant \gamma \leqslant 0.208$), in an attempt to study the onset of flow mixing. In their finite-volume numerical analysis, Asako and Faghri [8], and Yang et al. [10] have considered periodically developed steady laminar flow and heat transfer in corrugated channels of a triangular profile with sharp and rounded corners, and with walls maintained at a constant temperature. Metwally and Manglik [21,22] have considered periodically developed laminar flow and heat transfer in wavy-plate channels with spacing ratio $\varepsilon = 1.0$, and corrugation aspect ratios in the range of $0.25 \leqslant \gamma \leqslant 1.0$. In these studies, the wall waviness is found to induce steady flow re-circulation or lateral vortices in the trough regions of the corrugated-plate channel. The strength of these vortices increases with Reynolds number and severity of wall waviness γ, leading to substantial heat transfer enhancement in comparison with flows in a flat parallel-plate channel; the associated friction loss also increases. As seen in the triangular-profiled wavy channel results of Comini et al. [15], this performance is also affected by the relative inter-plate spacing. A detailed understanding of the compound effects of wall-waviness aspect ratio γ and inter-plate spacing ε on the swirl flow structure and its impact on forced convection is addressed in this paper, for the effective design and applications of sinusoidal wavy-plate fins.

The influence of the sinusoidal wavy-surface plate-fin geometry (γ and ε) on laminar airflow and convective heat transfer in the inter-fin channels is computationally investigated in this study. A two-dimensional flow

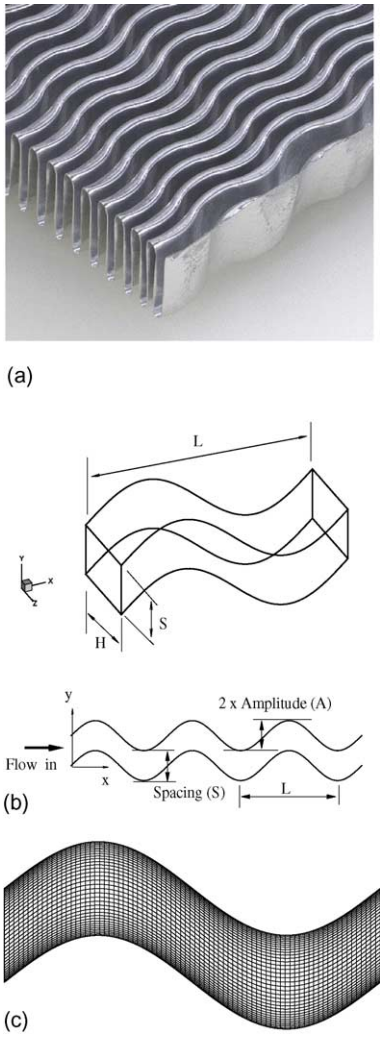

Fig. 1. Wavy-plate fins: (a) typical sinusoidally corrugated plate fins, (b) geometrical description and a two-dimensional representation of the inter-fin flow channel, and (c) typical non-uniform and non-orthogonal grid in the computational domain.

geometry ($H \gg S$, or $\alpha \to 0$) is considered, and the role of inter-fin spacing and severity of wall waviness in promoting the wall-curvature-induced periodically developed steady swirl flows is highlighted. With plate surfaces maintained at a uniform temperature (UWT condition) for the heat transfer problem, which is representative of conditions in refrigeration-to-air or turbulent liquid flow liquid-to-air exchangers, a wide range of air ($Pr = 0.7$) flow rates in the low Reynolds number regime ($10 \leqslant Re \leqslant 1000$) are considered. The local velocity and temperature distributions are mapped, and the parametric variations in the average isothermal Fanning friction factor f and Colburn factor j results with γ, ε, and Re are outlined along with an assessment of the enhanced thermal–hydraulic performance.

2. Formulation and computational methodology

A two-dimensional representation of the flow channel in a wavy-plate-fin core shown in Fig. 1(b) is considered, which is essentially obtained when the fin height is much larger than the inter-fin or inter-plate spacing ($H \gg S$; $\alpha \to 0$). For ease of computational modeling, the physical flow domain (x, y) is recast in generalized dimensionless body-fitted coordinates (ξ, η) that are defined as

$$\xi = (x/S), \quad \eta = [(y/S) - (A/S)\sin(2\pi S\xi/L)] \tag{1}$$

which render the wavy channel into a flat parallel-plate computational domain with unit inter-plate spacing.

The laminar airflow field ($Pr = 0.7$) is characterized by steady-state, constant property, periodically developed conditions, with negligible axial conduction ($Pe \gg 1$) and viscous dissipation ($Br \ll 1$). While there is some debate on whether steady-state conditions would exist as $Re \to 1000$ [11,24], several studies [16,18–21,25,26] have found substantial empirical evidence to suggest that steady flows do indeed prevail in most two-dimensional as well three-dimensional situations in wavy-wall channels to amply justify the present analysis assumption. In the computational domain (ξ, η), the dimensionless velocity components (U, V) are given by

$$U = (u/u_{\mathrm{m}}), \quad V = [(v/u_{\mathrm{m}}) - \omega U] \tag{2a}$$

where u_{m} is the mean axial velocity, and

$$\omega = (2\pi A/L)\cos(2\pi S\xi/L) \tag{2b}$$

Also, for periodically developed flows, the pressure field can be expressed as

$$p(x, y) = [p^*(x, y) - \beta x] \tag{3}$$

where β is the constant global pressure gradient, and p^* is the local pressure that exhibits periodicity, and their respective dimensionless forms are

$$B = (\beta S/\rho u_{\mathrm{m}}^2), \quad P = (p^*/\rho u_{\mathrm{m}}^2) \tag{4}$$

With the flow channel walls subjected to the uniform wall temperature boundary condition, which typically models the heat transfer condition in refrigerant-to-air evaporators and condensers, a dimensionless temperature can be defined as

$$\theta(x, y) = [T(x, y) - T_{\mathrm{w}}]/[T_{\mathrm{b}}(x) - T_{\mathrm{w}}] \tag{5}$$

Here $T_{\mathrm{b}}(x)$ is the local bulk or mixed-mean temperature, and $\theta(x, y)$ explicitly satisfies the periodic boundary condition over the one-period flow domain, $x = 0$ and L (Fig. 1(b)).

The dimensionless form of the mass conservation equation can therefore be expressed as

$$\frac{\partial U}{\partial \xi}+\frac{\partial V}{\partial \eta}=0 \tag{6}$$

and the momentum and energy transport equations can be written in the following generalized form:

$$U\frac{\partial \phi}{\partial \xi}+V\frac{\partial \phi}{\partial \eta}=\Gamma\left[\frac{\partial^2\phi}{\partial \xi^2}+(1+\omega^2)\frac{\partial^2\phi}{\partial \eta^2}\right]+S_\phi \tag{7}$$

Here $\phi = U$, V, and θ, respectively, and $\Gamma = (1/Re_S)$ for the momentum equations, and $[1/(Re_S Pr)]$ for the energy equation. The expressions for the respective source terms S_ϕ are as follows:

$$S_U=-\frac{1}{Re_S}\left[\frac{\partial}{\partial \xi}\left(\omega\frac{\partial U}{\partial \eta}\right)+\omega\frac{\partial}{\partial \eta}\left(\frac{\partial U}{\partial \xi}\right)\right]+B-\frac{\partial P}{\partial \xi}+\omega\frac{\partial P}{\partial \eta} \tag{8a}$$

$$S_V=-\frac{1}{Re_S}\left[\frac{\partial}{\partial \xi}\left(\omega\frac{\partial V}{\partial \eta}\right)+\omega\frac{\partial}{\partial \eta}\left(\frac{\partial V}{\partial \xi}\right)\right]+\omega\frac{\partial P}{\partial \xi}-(1+\omega^2)\frac{\partial P}{\partial \eta}+\frac{1}{Re_S}\left[2\frac{\partial \omega}{\partial \xi}\left(\frac{\partial U}{\partial \xi}-\omega\frac{\partial U}{\partial \eta}\right)+U\frac{\partial^2 U}{\partial \xi^2}\right]-\omega B-U^2\frac{\partial \omega}{\partial \xi} \tag{8b}$$

Table 1
Effect of grid refinement on f and j in a typical wavy-plate channel with $\gamma = 0.25$, and $\varepsilon = 1.0$ for flow with $Re = 250$

Mesh size	Friction factor f (% deviation)	Colburn factor j (% deviation)
50×25	0.13702	0.052139
60×35	0.13879 (1.29%)	0.052737 (1.15%)
80×45	0.13922 (0.31%)	0.053018 (0.53%)
100×55	0.13988 (0.47%	0.053124 (0.20%)
120×65	0.13997 (0.06%)	0.053167 (0.08%)

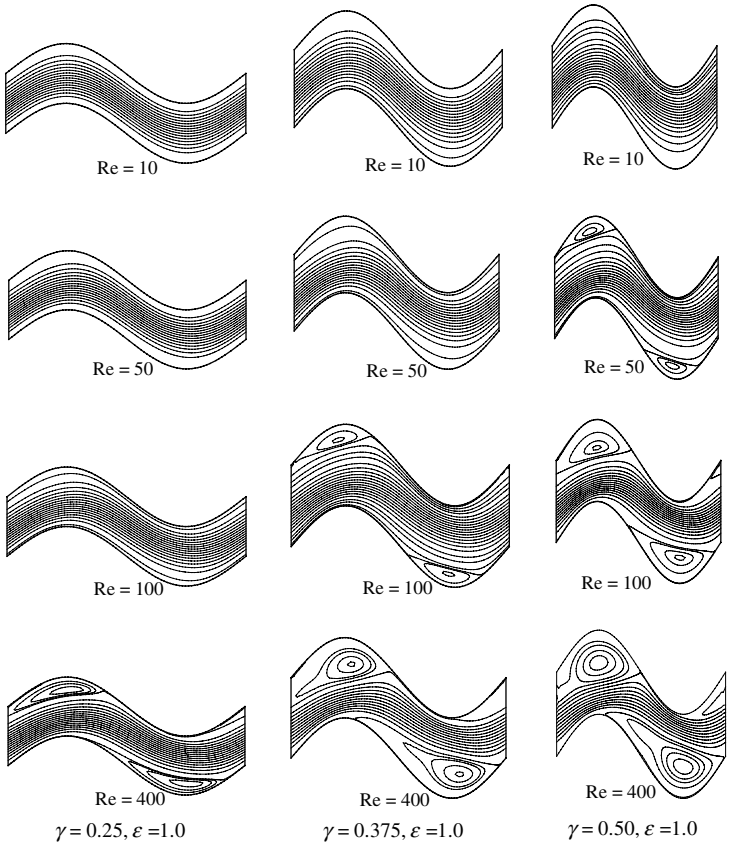

Fig. 2. Streamline distributions in wavy-plate channels with relative spacing of $\varepsilon = 1.0$ but different corrugation aspect ratio γ and flow Reynolds numbers.

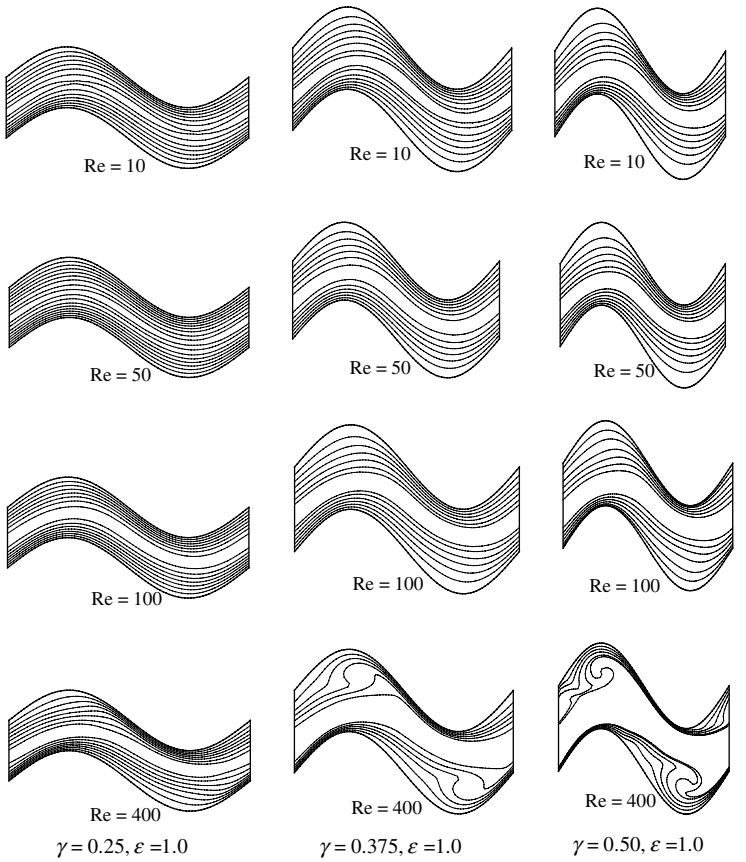

Fig. 3. Isotherm maps for air ($Pr = 0.7$) flows in wavy-plate channels with relative spacing of $\varepsilon = 1.0$ but different corrugation aspect ratio γ and flow Reynolds numbers.

$$S_\theta = -\frac{1}{Re_S Pr}\left[\frac{\partial}{\partial\xi}\left(\omega\frac{\partial\theta}{\partial\eta}\right)+\omega\frac{\partial}{\partial\eta}\left(\frac{\partial\theta}{\partial\xi}\right)\right] + \left[\frac{2}{Re_S Pr}\left(\frac{\partial\theta}{\partial\xi}-\omega\frac{\partial\theta}{\partial\eta}\right) - U\theta\right]\left[\frac{\mathrm{d}(T_b-T_w)/\mathrm{d}\xi}{(T_b-T_w)}\right] + \frac{\theta}{Re_S Pr}\left[\left(\frac{\mathrm{d}(T_b-T_w)/\mathrm{d}\xi}{T_b-T_w}\right)^2 + \frac{\mathrm{d}}{\mathrm{d}\xi}\left(\frac{\mathrm{d}(T_b-T_w)/\mathrm{d}\xi}{T_b-T_w}\right)\right] \tag{8c}$$

Also, U and V satisfy the no-slip and periodicity conditions, and θ satisfies the constant wall temperature and periodicity conditions. The latter essentially requires that

$$\phi(U,V,\theta)_{\xi=0} = \phi(U,V,\theta)_{\xi=1} \tag{9}$$

Finally, given the flow distribution, the one-period-length-averaged isothermal Fanning friction factor is obtained from its usual definition as

$$f = [-(\mathrm{d}p/\mathrm{d}x)(d_h/2\rho u_m^2)] = (Bd_h/2S) \tag{10}$$

The overall Nusselt number is computed from the temperature field by applying the energy balance over the one-period flow domain, and the log-mean temperature difference (LMTD) as

$$Nu = \frac{\dot{m}c_p(T_{b,o}-T_{b,i})d_h}{kA_h(\mathrm{LMTD})} = (A_c/A_h)(RePr)\left[-\int_0^L \frac{\mathrm{d}(T_b-T_w)/\mathrm{d}\xi}{(T_b-T_w)}\,\mathrm{d}x\right] \tag{11a}$$

where

$$T_b(x) = \left[\int |u|T(x,y)\,\mathrm{d}y \Big/ \int |u|\,\mathrm{d}y\right] \tag{11b}$$

$$\mathrm{LMTD} = \frac{(T_w-T_{b,o})-(T_w-T_{b,i})}{\ln[(T_w-T_{b,o})/(T_w-T_{b,i})]} \tag{11c}$$

The results, however, are presented in terms of the Colburn j factor ($Nu/RePr^{1/3}$), in conformity with the customary practice in the compact heat exchanger literature.

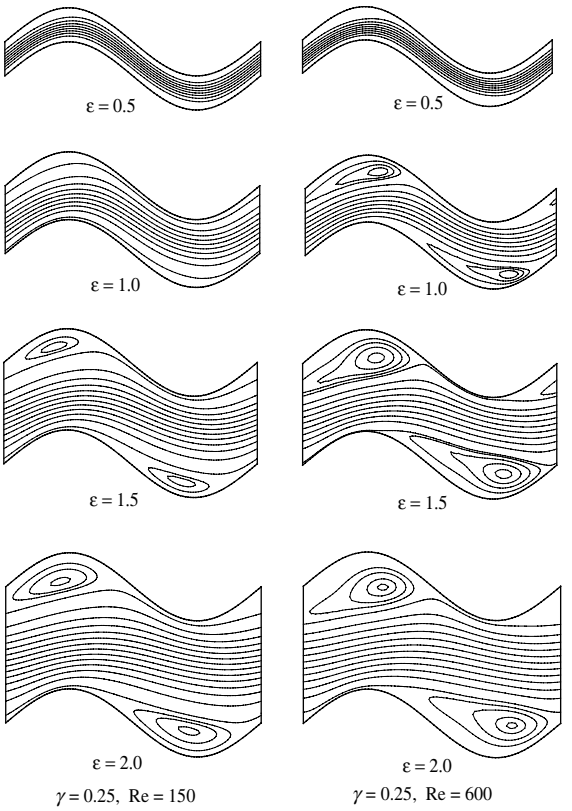

Fig. 4. Effect of ε on the streamline distribution on lateral swirl generation in wavy-plate channels with $\gamma = 0.25$, and $Re = 150$ and 600.

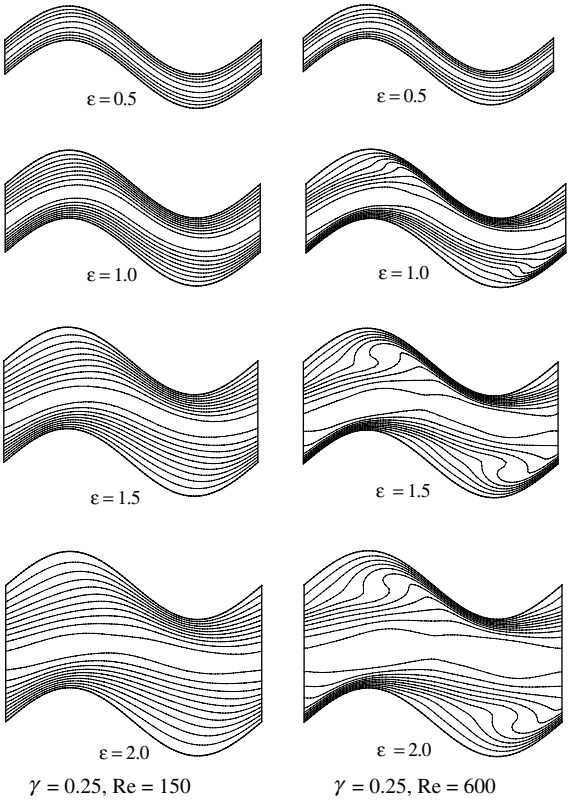

Fig. 5. Effect of ε and wall waviness-induced fluid re-circulation on the temperature field in wavy-plate channels with $\gamma = 0.25$, and air ($Pr = 0.7$) flow $Re = 150$ and 600.

To obtain numerical solutions, the governing differential equations were discretized on a structured, non-orthogonal grid using the finite-volume method. A typical computational mesh for the flow geometry is shown in Fig. 1(c), where the grid is uniform in the axial x or ξ direction, but non-uniform in the lateral y or η direction. The latter non-uniform mesh distribution is controlled by the following function:

$$\eta = a y_1 + (1 - a)\frac{1 - \tanh[b(1 - y_1)]}{\tanh(b)} \tag{12}$$

Here y_1 has a uniform distribution in the range $0 \leqslant y_1 \leqslant 1$, and the η distribution in the range $0 \leqslant \eta \leqslant 1$ is controlled by the two constraints a and b that were set as $a = 0.1$ and $b = 2.0$ in all simulations. This ensures a denser mesh near the walls for properly treating the high velocity and temperature gradients. Both the diffusion and convection terms are treated by the power-law differencing scheme, and the source terms by central differencing. The SIMPLE algorithm was applied to evaluate the coupling between the pressure and velocity [27]. For the periodically developed flow condition, as treated by Patankar et al. [28], the inlet–outlet periodicity of the flow velocity components and temperature field (normalized by the mean velocity and local bulk fluid temperature, respectively) were essentially imposed over a single corrugation module L in the streamwise direction as given by Eq. (9). The local bulk-mean temperature was obtained from Eq. (11b), with the numerical integration performed by a second-order accurate scheme. The mean velocity or flow Reynolds number was an a priori input, and the pressure gradient determined iteratively to satisfy the momentum conservation equations. Extended details of the computational methodology are given in Ref. [21,29].

The numerical results were first validated with analytical solutions for a parallel-plate flow channel, which is obtained by setting the amplitude $A = 0$ in the simulation. The computed values of $fRe = 24.05$ and $Nu = 7.529$ were within 0.2% of the exact analytical results of 24.0 and 7.541, respectively. To determine the proper grid size required for numerical simulation, grid refinement experiments were performed. As an illustrative example, for the case of $Re = 250$, $\gamma = 0.25$, and $\varepsilon = 1.0$, the f and j results for five different mesh sizes

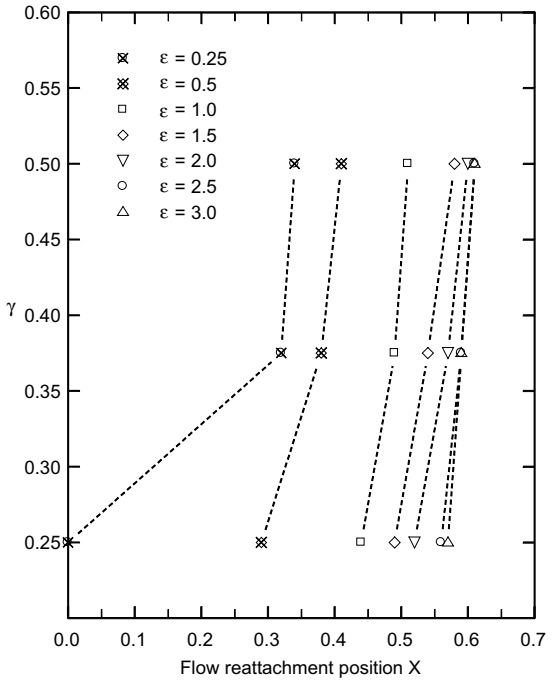

Fig. 6. Position of re-attachment point for different ε and γ at $Re = 600$ for core-flow development.

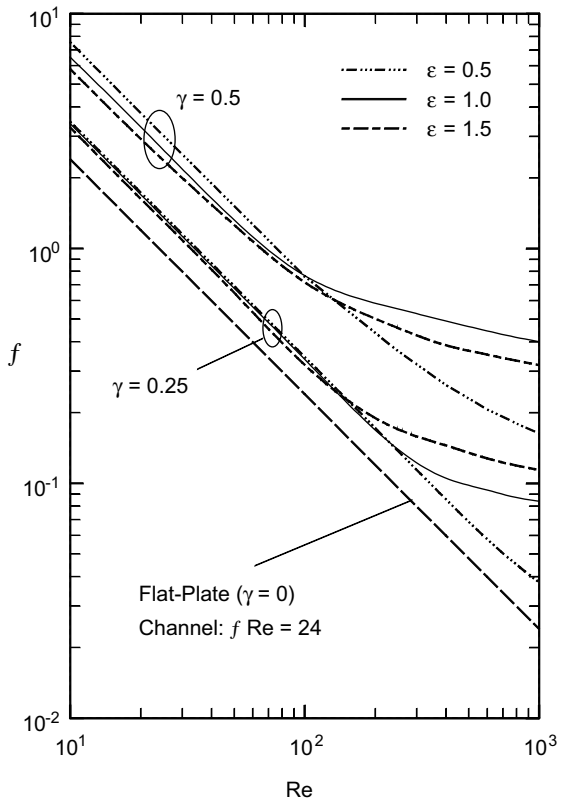

Fig. 7. Isothermal Fanning friction factors for periodically developed laminar airflows in sinusoidal wavy-plate channels.

are listed in Table 1. It can be seen that the relative errors with successive mesh refinement decrease to less than 0.1%, and a 100×55 grid is adequate for this case. Similar grid-refinement experiments were carried out for a few other cases, and the final grid sizes used in the simulations typically ranged from 100×35 for $\gamma = 0.25$ and $\varepsilon = 0.5$, to 120×115 for $\gamma = 0.5$ and $\varepsilon = 3.0$; more details can be found in Ref. [29]. Furthermore, the computed $f\,Re$ results for $0.25 \leqslant \gamma \leqslant 0.5$ are within $\pm1.2\%$ of those previously reported for the specific case of $\varepsilon = 1.0$, modeled for flow passages in chevron-plate type plate-and-frame heat exchangers [21].

3. Results and discussion

Numerical results for the velocity and temperature fields, isothermal Fanning friction factor, Colburn factor, and their variation with flow Reynolds number in different wavy-plate channels ($0.125 \leqslant \gamma \leqslant 0.5$, and $0.1 \leqslant \varepsilon \leqslant 3.0$) are presented. The influence of the flow geometry on the local velocity and temperature distribution, and the nature of wavy-surface-induced lateral vortex structure are delineated, along with an evaluation of the enhanced thermal–hydraulic performance.

The onset, development, and growth of steady lateral vortices or re-circulation in the troughs of wavy plate channels with changing flow rates are depicted in Fig. 2. Streamlines for flows with $Re = 10$, 50, 100, and 400 in three different wavy-fin geometries with $\varepsilon = 1.0$, and $\gamma = 0.25$, 0.375, and 0.5 are graphed, and the strong influences of Re and severity of wall waviness γ are clearly evident. With increasing flow rates, wall-curvature-induced effects manifest in fluid separation downstream of the wavy-surface peak, its re-attachment upstream of the subsequent peak, and the consequent development and encompassing of re-circulating cells in the wall-valley regions. This lateral vortex is triggered at a much lower flow rate in channels with more severe wall waviness ($Re \sim 50$ with $\gamma = 0.5$, as compared to $Re > 100$ with $\gamma = 0.25$; $\varepsilon = 1.0$ in both cases), and the extent of the lateral swirl flow area coverage increases with Re and γ. At very low flow rates ($Re \sim 10$), however, viscous forces dominate to produce undisturbed streamline flows and swirl is not developed, irrespective of the wall-corrugation severity γ. The corresponding impact on the local convective temperature distribution in airflows ($Pr = 0.7$) between uniform temperature plates is illustrated by the isotherm plots of Fig. 3. With the development of trough-region re-circulation, there is considerable thinning of the boundary layer and the flow field exhibits regions of thermal mixing. Also, the

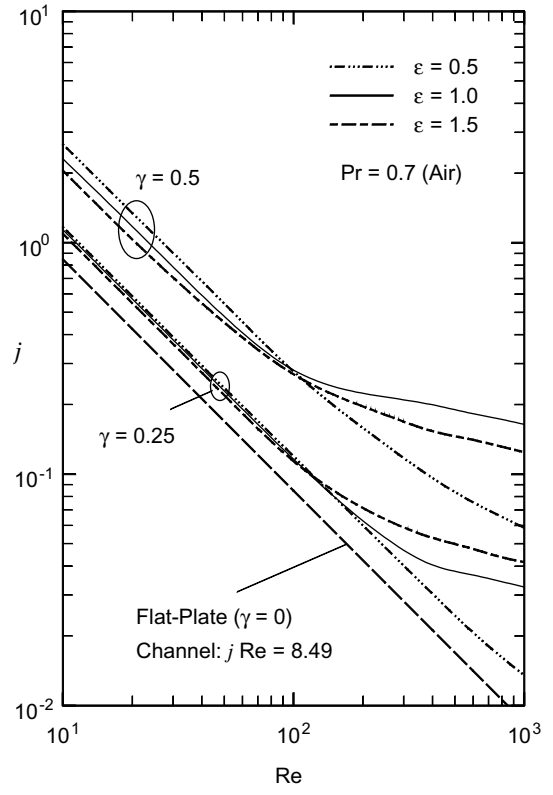

Fig. 8. Colburn factors for periodically developed laminar airflows in sinusoidal wavy-plate channels with constant wall temperature.

increasing spatial coverage of the trough vortices with Re and γ results in more uniform core region temperature distributions, and much sharper wall temperature gradients.

That the inter-plate-fin spacing, represented by the dimensionless ε $(=S/2A)$, significantly influences the development of flow re-circulation in the wavy-wall valleys is seen from the streamlines graphed in Fig. 4. The flow fields for $Re = 150$ and 600 in channels with $\gamma = 0.25$, and $0.5 \leqslant \varepsilon \leqslant 2.0$ are depicted. With increasing Re and/or plate spacing ε, the lateral vortex in the trough tends to grow and envelop much of the core flow region, thereby promoting flow mixing and increased momentum transport. As the plate separation decreases ($\varepsilon \to 0.5$), viscous effects suppress swirl and undisturbed streamline flows prevail that follow the channel-wall contours. This flow behavior, however, depends on both ε and Re for any given γ. As seen in Fig. 4 for flows in a $\gamma = 0.25$ channel, swirl sets in with $\varepsilon = 1.0$ and $Re = 600$ but not $Re = 150$; in the latter case, trough-region re-circulation occurs only when $\varepsilon > 1.0$. Similarly, the airflow ($Pr = 0.7$) temperature distributions in Fig. 5 reflect a fully developed duct flow like condition in cases where ε is small. With increasing ε or Re and the attendant development of lateral vortices, on the other hand, the temperature field displays a periodicity that is characterized by local regions of considerably thin thermal boundary layers, resulting in the local heat transfer performance enhancement. The temperature distribution in the core flow becomes more uniform with the growth of swirl, and the overall convection heat transfer increases.

There is, however, an upper limit to the effect of ε in promoting swirl enhancement. With increasing ε the influence of wall waviness on the bulk flow and heat transfer diminishes significantly, and this can be also deduced from Fig. 6. Here the position of the axial flow re-attachment points, demarking in effect the separated wall-trough region that envelopes the lateral vortex, are graphed for different ε and γ in typical swirl regime flows with $Re = 600$. For the same wall waviness γ, the re-attachment points move axially to the right with increasing ε thereby indicating growth of the separated region. But after a critical ε, they remain at the same position as the size of the separated region remains constant and is unaffected by further increase in the inter-plate separation.

The variation of isothermal Fanning friction factors with Re and the wavy-channel geometry (γ and ε) are presented in Fig. 7. Results for channels with $\gamma = 0.25$ and 0.5, and $0.25 \leqslant \varepsilon \leqslant 1.5$ are graphed, along with that for a flat-plate channel ($\gamma = 0$, $f\,Re = 24$, [30]). The friction factor is seen to increase with the severity of wall corrugation ($\gamma = 0.25 \to 0.5$), and Re. The onset and steady spatial growth of periodically developed lateral vortices in the trough regions of the wavy plate can be deduced from the slope change in the f–Re plot. Two distinct regimes can be identified: (i) swirl flow regime as $Re \to 1000$ and/or γ increases, and (ii) streamline flow regime as $\gamma \to 0$ and/or Re decreases. The greater magnitude and extent of the wall-trough region re-circulation when the plate separation is larger ($\varepsilon = 0.5 \to 1.5$), which result in higher wall shear stress in the swirl regime is also evident from the higher f values in Fig. 7. This increase in f, however, is not uniform across varying severity of wall waviness γ. For example, while f increases with ε for all $Re > 100$ and $\gamma = 0.25$, with $\gamma = 0.5$ it is seen to increase as $\varepsilon = 0.5 \to 1.0$ and then decrease when $\varepsilon = 1.5$. In the viscous-forces dominated no-swirl regime ($Re \sim O$ [10]), on the other hand, ($f\,Re$) is constant and decreases monotonically with increasing ε.

The concomitant influence of the altered flow structure in wavy-plate ducts on the period-averaged heat transfer coefficient is depicted in Fig. 8, where the variations in the Colburn j factors with Re, γ, and ε are presented for airflows ($Pr = 0.7$). Included is the result for fully developed laminar flow in a parallel flat-plate channel given by $Nu = 7.541$ ($j\,Re = 8.493$ for $Pr = 0.7$)

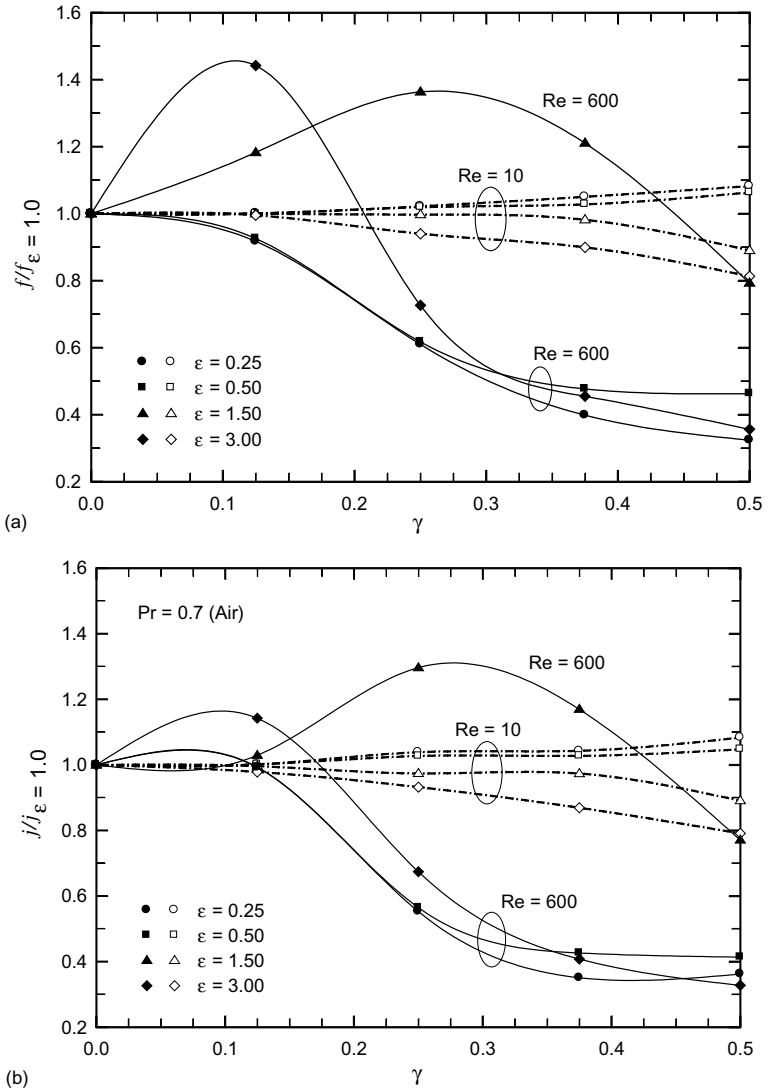

Fig. 9. Effect of fin spacing on the (a) normalized friction factor, and (b) normalized Colburn factor at different flow rates.

for the constant wall temperature condition [30]. In the presence of the wall-trough region lateral swirl and the associated improvement in fluid convection, the overall heat transfer coefficient is seen to enhance significantly with increasing γ and ε in the $Re > 100$ regime. In the low flow rate ($Re \sim 0$ [10]) regime, just as its frictional loss counterpart, (jRe) is also constant and the heat transfer enhancement is mainly due to the increased effective surface area and larger residence time provided by the corrugated plate channel. Again, the combined interplay of ε, γ, and Re is similar to that seen in the friction factor results, with effects of increasing/decreasing ε modulated by γ and Re.

The somewhat complex effects of channel spacing ε on the flow frictional loss and heat transfer coefficient are further highlighted in Fig. 9. The values for f and j in different γ channels, normalized by the corresponding results with $\varepsilon = 1.0$ are graphed. In the no-swirl regime ($Re = 10$), the decreasing impact of the interactions between viscous and wall-curvature-induced forces in the confined wavy-flow passages is evident in Fig. 9(a) from the reduction in f with increasing ε for all γ. As would be expected the greatest effect is seen in channels with more severely corrugated ($\gamma \to 0.5$) plates. The normalized Colburn factor ($j/j_{\varepsilon=1.0}$) results also display a similar behavior in Fig. 9(b). In the swirl regime ($Re = 600$), on the other hand, the trends are quite different and $f(\varepsilon < 1) \leqslant f(\varepsilon = 1)$ for all γ; the corresponding j though tends to be slightly higher for $0 < \gamma < 0.125$. When $\varepsilon > 1$ and depending upon γ, ($f/f_{\varepsilon=1.0}$) first increases with ε

and then decreases. With $\varepsilon = 3.0$, for example, f peaks in $\gamma \sim 0.1$ channels, and then decreases considerably with increasing γ. The degradation in f is most pronounced in $\gamma = 0.5$ channels, where $f_{\varepsilon=3.0}$ is even less than $f_{\varepsilon=0.5}$. This reduction is perhaps due to diminishing wall curvature effects as the inter-plate spacing increases, whereby the lateral vortex ceases to grow spatially and the core flow remains relatively undisturbed. Likewise, the Colburn factor ratio ($j/j_{\varepsilon=1.0}$) displays similar trends as seen in Fig. 9(b).

A closer inspection of the thermal–hydraulic performance reveals that the heat transfer coefficient is enhanced by up to 7.75 times that in a flat-plate channel, whereas the associated pressure drop penalty is only 6.8 times higher in a typical wavy-plate channels with $\gamma = 0.375$. This relative thermal advantage with different γ and ε can be better depicted by the *area goodness factor* [3,30], given by the following ratio:

$$(j/f) = (Nu\,Pr^{-1/3}/f\,Re) \tag{13}$$

which is a measure of the relative compactness of the enhanced heat transfer surface. This is depicted in Fig. 10, where the wavy-fin ($\gamma = 0.25$, 0.375, and 0.5) performance with $0.1 \leqslant \varepsilon \leqslant 3.0$ is graphed for both the swirl-flow ($Re = 600$) and no-swirl ($Re = 10$) regimes along with the flat-fin ($\gamma = 0$) performance. The enhancement in the swirl region is clearly evident for all values of γ and $\varepsilon > 0$. The relative thermal–hydraulic performance improves considerably with increasing γ, and an optimum is attained when $1.0 < \varepsilon < 1.2$. In the no-swirl region ($Re \sim 10$), however, the relatively larger surface area of the wavy fin does not produce any effective enhancement, when compared with the performance of plain flat fins.

4. Conclusions

Low Reynolds number, periodically developed airflow and heat transfer ($Pr = 0.7$) in uniform-wall-temperature, sinusoidal wavy-plate channels are modeled. Numerical results for a wide range of steady laminar flows ($10 \leqslant Re \leqslant 1000$) and duct-geometry variations ($0.125 \leqslant \gamma \leqslant 0.5$, and $0.1 \leqslant \varepsilon \leqslant 3.0$) are presented. The wavy-wall curvature induces lateral vortices in the trough region, which grow in magnitude and spatial flow coverage with increasing Re and/or γ. The inter-plate separation, however, is critical for the development of this flow structure. With small separation ($\varepsilon \leqslant 0.5$), viscous forces dominate and a streamline, fully developed duct flow type behavior prevails. With larger inter-plate gap ($\varepsilon \geqslant 1.0$), this effect diminishes and the boundary-layer separation downstream of corrugation peaks gives rise to a vortex flow structure in the valley region. The re-circulation is enveloped in the near-wall axial flow separation bubble, and its spatial growth is governed by Re, γ, and ε. The consequent local fluid mixing and core-flow acceleration results in enhanced convective heat transfer, though the associated flow friction also increases.

The $(f - Re)$ and $(j - Re)$ results suggest two distinct flow regimes: (1) a low-Re ($Re \to 10$) regime with fully developed streamline flows, and (2) a high-Re ($Re \to 1000$) regime that is characterized by lateral vortices in the wall corrugation troughs. The heat transfer performance in the swirl flow regime ($Re \sim 600$) is found to be enhanced considerably for all γ and $\varepsilon > 0.25$, when compared with the (j/f) performance of flat fins, and a peak performance is obtained with $1.0 < \varepsilon < 1.2$. In low flow rates ($Re \sim 10$), on the other

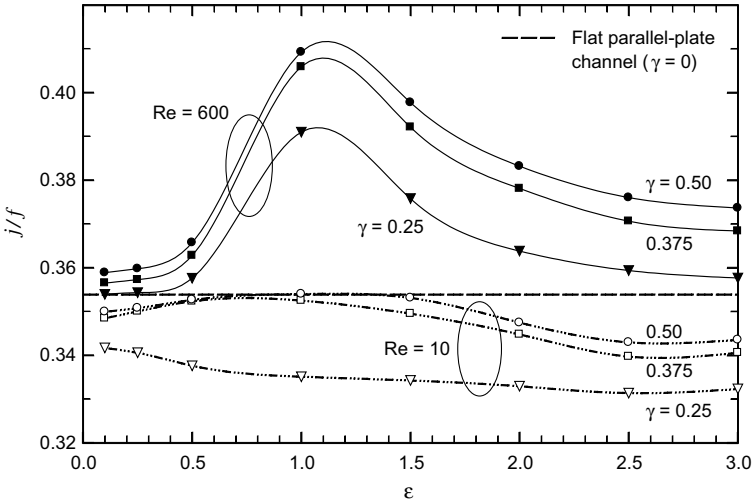

Fig. 10. Heat transfer enhancement in the swirl-flow ($Re = 600$) and no-swirl flow ($Re = 10$) regimes on a constant pumping power basis, and the effect of plate separation.

hand, a much larger fin waviness severity ($\gamma > 0.5$) may be required in order to achieve any significant enhancement.

Acknowledgements

This study was supported in part by Honeywell Engines & Systems, the National Science Foundation (Grant # CTS-9502128), and the University Research Council. Also, the advice and support of Dr. A. Muley, Mr. J.B. Borghese, and Dr. H. Strumpf are gratefully acknowledged.

References

[1] W.M. Kays, A.L. London, Compact Heat Exchangers, third ed., McGraw-Hill, New York, 1984.
[2] A.E. Bergles, Techniques to enhance heat transfer, in: W.M. Rohsenow, J.P. Hartnett, Y.I. Cho (Eds.), Handbook of Heat Transfer, third ed., McGraw-Hill, New York, 1998 (Chapter 11).
[3] R.M. Manglik, Heat transfer enhancement, in: A. Bejan, A.D. Kraus (Eds.), Heat Transfer Handbook, Wiley, New York, 2003 (Chapter 14).
[4] R.M. Manglik, A.E. Bergles, Heat transfer and pressure drop correlations for the rectangular offset-strip-fin compact heat exchanger, Exp. Therm. Fluid Sci. 10 (2) (1995) 171–180.
[5] R.L. Webb, Principles of Enhanced Heat Transfer, Wiley, New York, 1994.
[6] R.K. Shah, Heat exchangers, in: W.M. Rohsenow, J.P. Hartnett, Y.I. Cho (Eds.), Handbook of Heat Transfer, McGraw-Hill, New York, 1998 (Chapter 17).
[7] K. Vajravelu, Fluid flow and heat transfer in horizontal wavy channels, Acta Mech. 35 (1980) 245–258.
[8] Y. Asako, M. Faghri, Finite-volume solutions for laminar flow and heat transfer in a corrugated duct, J. Heat Transfer 109 (3) (1987) 627–634.
[9] V.K. Garg, P.K. Maji, Flow and heat transfer in a sinusoidally curved channel, Int. J. Eng. Fluid Mech. 1 (3) (1988) 293–319.
[10] L.C. Yang, Y. Asako, Y. Yamaguchi, M. Faghri, Numerical predication of transitional characteristics of flow and heat transfer in a corrugated duct, J. Heat Transfer 119 (1) (1997) 62–69.
[11] T.A. Rush, T.A. Newell, A.M. Jacobi, An experimental study of flow and heat transfer in sinusoidal wavy passages, Int. J. Heat Mass Transfer 42 (1999) 1541–1553.
[12] J. Zhang, R.M. Manglik, A. Muley, J.B. Borghese, Three-dimensional numerical simulation of laminar air flows in wavy plate-fin channels, in: Proceedings of 13th International Symposium on Transport Phenomena (ISTP –13), Victoria, BC, Canada, July 14–18, 2002.
[13] J. Min, R.L. Webb, Numerical predications of wavy fin coil performance, J. Enhanced Heat Transfer 8 (3) (2001) 159–173.
[14] G. Comini, C. Nonino, S. Savino, Convective heat and mass transfer in wavy finned-tube exchangers, Int. J. Numer. Methods Heat Fluid Flow 12 (2) (2002) 735–755.
[15] G. Comini, C. Nonimo, S. Savino, Effect of space ratio and corrugation angle on convection enhancement in wavy channels, Int. J. Numer. Methods Heat Fluid Flow 13 (4) (2003) 500–519.
[16] T. Nishimura, Y. Ohori, Y. Kajimoto, Y. Kawamura, Mass transfer characteristics in a channel with symmetric wavy wall for steady flow, J. Chem. Eng. Jpn. 18 (6) (1985) 550–555.
[17] T. Nishimura, Y. Kajimoto, Y. Kawamura, Mass transfer enhancement in channels with a wavy wall, J. Chem. Eng. Jpn. 19 (2) (1986) 142–144.
[18] T. Nishimura, S. Murakami, S. Arakawa, Y. Kawamura, Flow observation and mass transfer characteristics in symmetrical wavy-walled channels at moderate Reynolds number for steady flow, Int. J. Heat Mass Transfer 33 (5) (1990) 835–845.
[19] W.W. Focke, J. Zachariades, I. Olivier, The effect of the corrugation inclination angle on the thermo-hydraulic performance of plate heat exchangers, Int. J. Heat Mass Transfer 28 (8) (1985) 1469–1479.
[20] D. Béreiziat, R. Devienne, M. Lebouché, Local flow structure for non-Newtonian fluids in a periodically corrugated wall channel, J. Enhanced Heat Transfer 2 (1–2) (1995) 71–77.
[21] H.M. Metwally, R.M. Manglik, Numerical solutions for periodically-developed laminar flow and heat transfer in sinusoidal corrugated plate channels with constant wall temperature, in: Proceedings of 2000 National Heat Transfer Conference, Paper No. NHTC2000-12216, ASME, New York, 2000.
[22] H.M. Metwally, R.M. Manglik, A computational study of enhanced heat transfer in laminar flows of non-Newtonian fluids in corrugated-plate channels, in: R.M. Manglik, T.S. Ravigururajan, A. Muley, R.A. Papar, J. Kim (Eds.), Advances in Enhanced Heat Transfer, HTD-vol. 365/PID-vol. 4, ASME, New York, 2000, pp. 41–48.
[23] C. Zimmerer, P. Gschwind, G. Gaiser, V. Kottke, Comparison of heat and mass transfer in different heat exchanger geometries with corrugated walls, Exp. Therm. Fluid Sci. 26 (2002) 269–273.
[24] T. Nishimura, K. Yano, T. Yoshino, Y. Kawamura, Occurrence and structure of Taylor–Goertler vortices induced in two-dimensional wavy channels for steady flow, J. Chem. Eng. Jpn. 23 (6) (1990) 697–703.
[25] A. Muley, R.M. Manglik, H.M. Metwally, Enhanced heat transfer characteristics of viscous liquid low Reynolds number flows in a chevron plate heat exchanger, J. Heat Transfer 121 (4) (1999) 1011–1017.
[26] A. Muley, J. Borghese, R.M. Manglik, J. Kundu, Experimental and numerical investigation of thermal-hydraulic characteristics of wavy-channel compact heat exchanger, in: Heat Transfer—2002, Proceedings of 12th International Heat Transfer Conference, vol. 4, Société Française des Thermiciens & Elsevier, France, 2002.
[27] S.V. Patankar, Numerical Heat Transfer and Fluid Flow, Hemisphere, New York, 1980.
[28] S.V. Patankar, C.H. Liu, E.M. Sparrow, Fully developed flow and heat transfer in ducts having streamwise-periodic

variations of cross-sectional area, J. Heat Transfer 99 (1977) 180–186.

[29] J. Kundu, R.M. Manglik, Numerical investigation of laminar forced convection in two-dimensional and three-dimensional sinusoidal corrugated ducts, Thermal-fluids & Thermal Processing Laboratory Report No. TFTPL-5, University of Cincinnati, Cincinnati, OH, 2000.

[30] R.K. Shah, A.L. London, Laminar Flow Forced Convection in Ducts, Supplement 1 to Advances in Heat Transfer, Academic, New York, NY, 1978.